Potential Energy Surface for the F(2 P 3/2 , 2 P 1/2) + CH 4 Hydrogen Abstraction Reaction. Kinetics and Dynamics Study

ARTICLE *in* THE JOURNAL OF PHYSICAL CHEMISTRY A · MARCH 2005

Impact Factor: 2.69 · DOI: 10.1021/jp044765v · Source: PubMed

3 AUTHORS:

Cipriano Rangel
Universidad de Extremadura
27 PUBLICATIONS **321** CITATIONS
SEE PROFILE

Marta Navarrete
Spanish National Research Council
22 PUBLICATIONS **1,237** CITATIONS
SEE PROFILE

Joaquin Espinosa-Garcia
Universidad de Extremadura
141 PUBLICATIONS **2,186** CITATIONS
SEE PROFILE

Potential Energy Surface for the $F(^2P_{3/2},^2P_{1/2}) + CH_4$ Hydrogen Abstraction Reaction. Kinetics and Dynamics Study

Cipriano Rángel, Marta Navarrete, and J. Espinosa-García*

Departamento de Química Física, Universidad de Extremadura, 06071 Badajoz, Spain

Received: November 16, 2004; In Final Form: December 14, 2004

A modified and recalibrated potential energy surface (PES) is reported for the gas-phase $F(^2P_{3/2},^2P_{1/2}) + CH_4$ reaction and its deuterated analogue. This semiempirical surface is completely symmetric with respect to the permutation of the four methane hydrogen atoms and is calibrated with respect to the updated experimental and theoretical stationary point properties and experimental thermal rate constants. To take into account the two spin−orbit electronic states of the fluorine atom, two versions of the surface were constructed, the PES−SO and PES−NOSO surfaces, which differ in the choice of the zero reference level of the reactants. On both surfaces, the thermal rate constants were calculated using variational transition-state theory with semiclassical transmission coefficients over a wide temperature range, 180−500 K. While the PES−SO surface overestimates the experimental rate constants, the PES−NOSO surface shows a better agreement, reproducing the experimental variation with temperature. The influence of the tunneling factor is negligible, due to the flattening of the surface in the entrance valley, and we found a direct dependence on temperature, and therefore positive and small activation energies, in agreement with experiment. The kinetic isotope effects calculated showed good agreement with the sparse experimental data at 283 and 298 K. Finally, on the PES−NOSO surface, other dynamical features, such as the coupling between the reaction coordinate and the vibrational modes, were analyzed. It was found qualitatively that the FH stretching and the CH_3 umbrella bending modes in the products appear vibrationally excited. These kinetics and dynamics results seem to indicate that a single, adiabatic PES is adequate to describe this reaction.

1. Introduction

The construction of new analytical potential energy surfaces (PES) for the kinetics and dynamics description of polyatomic reactive systems is a process in continuous evolution, intimately related with the development of high-level theoretical methods, functional forms better suited to representing the nuclear motion, and the appearance of new experimental data. Clearly, such continuous updating is a common process in science. A paradigmatic example has been the construction of the PES for the polyatomic system $CH_4 + H$ in the same way as the $H_2 + H$ system has been the paradigm of triatomic reactions.

In 1996, our group[1] reported for the first time an analytical PES for the title reaction. Our rate constant calculations and the kinetic isotope effects (KIEs) using canonical variational transition-state theory with small-curvature tunneling transmission coefficients agreed reasonably with the available experimental data, and from a dynamics point of view, we found that, while the vibrational excitation of the FH product is important, that of the CH_3 fragment is small or negligible. However, this 1996 PES presented two major shortcomings, one in the calibration process, and another in the asymmetric character of the overall functional forms, that we shall now comment on. With respect to the first point, in the 1996 paper we used as calibration criteria experimental data from two sources,[2,3] which present contradictory results. While the Atkinson et al. data[2] indicate that the rate constant increases with temperature, the Moore et al. results[3] have the inverse behavior, i.e., the rate constants diminish with temperature. Several theoretical[4−9] and experimental[10−17] works have appeared since then, making a new calibration necessary for kinetics and dynamics studies. The most recent kinetics results confirm the Atkinson et al.'s temperature dependence. With respect to the second point, the PES used in our previous work was based on the CH_5 PES of Joseph et al.[18] and basically consisted of four London−Eyring−Polanyi (LEP) functions augmented by bending terms. Jordan and Gilbert[19] for the same CH_5 system noted that while the LEP functional forms were symmetric to all four methane hydrogens, some bending terms were not symmetric. Later, our group[20] noted that neither was the Jordan and Gilbert PES completely symmetric in all the potential energy terms pertaining to the four methane hydrogen atoms, i.e., the surface was dependent on the input data. In this line, we have recently developed PESs symmetric with respect to the four methane hydrogens for the kinetics and dynamics description of similar hydrogen abstraction reactions with methane, $O(^3P)+CH_4$,[21] $Cl+CH_4$,[22] $OH+CH_4$,[23] $Br+CH_4$,[25] and $H+CH_4$.[25]

In the present paper, we use this knowledge to build the analytical symmetric PES for the $F(^2P_{3/2},^2P_{1/2}) + CH_4(X\ ^1A_1) \rightarrow FH(X\ ^1\Sigma^+) + CH_3(X\ ^2A''_2)$ gas-phase reaction based on the analytical symmetric PES for the $H + CH_4 \rightarrow H_2 + CH_3$ reaction previously developed by our group.[25] The title reaction presents several important features that invite theoretical study. Because of the very large exothermicity ($\Delta H_r^\circ = -32.0$ kcal mol^{-1}), the reaction path is very difficult to calculate because of a very flat PES, and the kinetics data are of especial interest because of the FH(v) vibrational population inversion produced in this reaction.[26] The paper is organized as follows. In section 2, the new symmetric PES is developed and calibrated, and section 3 presents the computational details describing the reaction-path analysis, variational transition-state theory (VTST),

10.1021/jp044765v CCC: $30.25
Published on Web 01/28/2005

and tunneling methods. The results of the VTST calculations are presented in section 4 and compared to experimental values and other theoretical results. This section also contains some KIEs for the deuterated analogue reaction and a comparison with our previous asymmetric PES (APES). The conclusions are presented in section 5.

2. PES

It is well-known that the complete construction of an analytical PES is no trivial task and is time-consuming. Basically, two phases can be considered in its construction. In a first phase, the functional forms to represent the stretching and bending modes must be chosen; in the second phase, a calibration with respect to updated theoretical and experimental data must be carried out.

2.1. Functional Forms. The new PES for the $F + CH_4 \rightarrow FH + CH_3$ reaction is based on the symmetric PES for the similar hydrogen abstraction reaction from methane, $H + CH_4 \rightarrow H_2 + CH_3$, previously reported by our group.[25] Briefly, the new surface is formulated in terms of stretching (str), valence (val) bending, and out-of-plane (op) bending terms and has the form

$$V = V_{str} + V_{val} + V_{op} \tag{1}$$

where V_{str} is the stretching term given by

$$V_{str} = \sum_{i=1}^{4} V_3(R_{CHi},R_{CF},R_{CH}) \tag{2}$$

and where V_3 represents the LEP functional form. The bending terms (V_{val} and V_{op}) are designed to be reasonable both for the methane molecule and for the methyl radical. The mathematical expressions for these terms are given in the original papers[18,19,25] and are not repeated here; although to make the reading easier, we shall comment on some parameters used in the calibration process. The term V_3 involves a singlet curve depending on three parameters ($^1D_{X-Y}$, α_{X-Y}, and R^e_{X-Y}) and a triplet curve depending on five parameters ($^3D_{X-Y}$, β_{X-Y}, c_{X-Y}, a_{X-Y}, and R^e_{X-Y}) for each bond X−Y. It is important to note that all three terms in eq 1, V_{str}, V_{val}, and V_{op}, are now symmetric and independent of the order of the hydrogens, and therefore the new PES is symmetric with respect to the permutation of the methane hydrogen atoms, a feature that is especially interesting for dynamics calculations.

2.2. Calibration of the Analytical PES. Having selected the functional form, the following step is to calibrate the surface, i.e., all the properties (geometry, vibrational frequency, energy, and forward rate constants) considered as a whole. The calibration process used in this work has several iterative steps. In the first step, we change the parameters (R^e_{X-Y}, $^1D_{X-Y}$, α_{C-H}, α_{C-F}) of the PES related to the geometric, energy, and vibrational properties of the reactants and products, so that the geometries, energies, and vibrational frequencies agree reasonably with the available experimental values. In a second step, we refit some parameters ($^3D_{X-Y}$, α_{C-F}) in order to reproduce the characteristics of the ab initio calculated saddle point (geometry, vibrational frequencies, and barrier height).

Finally, since one objective of this work was to explain the whole set of experimental forward rate constants, as the third step of our calibration, we refit some of the parameters of the analytical surface to calibrate it against the most recent experimental values.[10b,17] However, in this case it is necessary to take into account two issues. First, the error bars in the experimental measurements are important. The experimental study of Persky[10a] reported the expression $1.64 \times 10^{-10}(\pm 5 \times 10^{-12})$ $\exp(-265 \pm 10/T)$, cm^3 $molecule^{-1}$ s^{-1} over the temperature range 184−406 K. For instance, at 300 K, the rate constant ranges between 6.30×10^{-11} and 7.00×10^{-11}, with a recommended value of 6.65×10^{-11} cm^3 $molecule^{-1}$ s^{-1}. On the basis of this information, the most recent review of experimental information of Atkinson et al.[17] suggests the expression $1.3 \times 10^{-10} \exp(-215 \pm 200/T)$ over the range 180−410 K, with a larger error bar. For instance, at 300 K, the rate constant ranges from 3.25×10^{-11} to 12.3×10^{-11}, with a recommended value of 6.35×10^{-11} cm^3 $molecule^{-1}$ s^{-1}, close to the most recent recommended value of Persky.[10b]

Second, the F atom presents two spin−orbit electronic states, $^2P_{3/2}$ and $^2P_{1/2}$, which are split by only 404 cm^{-1} (1.15 kcal mol^{-1}). A priori, there is the possibility of reaction from these two states. Unfortunately, there are no theoretical relativistic studies on this reaction, and a study of this type is beyond the scope of the present work. We shall therefore take the similar and very well studied $F(^2P_{3/2},^2P_{1/2}) + H_2$ atom−diatom reaction for comparison purposes (see, for instance, ref 27 for the most recent studies). Alexander et al.[27a,c] found, first, that the reactivity of the excited s−o state of F is small, 10−25% of the reactivity of the ground s−o state, and second that the overall dynamics of the $F + H_2$ reaction will be well described by calculations on a single, electronically adiabatic PES. We assume this same behavior for the similar $F + CH_4$ reaction.

Therefore, considering this s−o effect, the electronic partition function for the reactants takes the usual expression

$$Q_e = 4 + 2\exp(-\epsilon/k_BT) \tag{3}$$

where ϵ is the s−o splitting of the fluorine atom, i.e., we are taking as reference level the s−o ground state of the fluorine atom ($^2P_{3/2}$). This surface will be denoted PES−SO, adiabatic PES including empirically the s−o effect in reactants.

The final functional form and the adjustable parameters for the new PES−SO surface are given on our Web page.[28] Note that this surface is semiempirical, in the sense that experimental and theoretical information is used to calibrate it.

The results of the final fit are listed in Table 1 for reactants and products and in Table 2 for the saddle point. In general, the reactant and product properties (the only properties directly comparable with experiment) show reasonable agreement with experiment,[29] with the most significant difference being 0.02 Å for the C−H bond length in CH_3. The agreement with the experimental exothermicity of the reaction, $\Delta H_r°(0\ K) = -32.0 \pm 0.5$ kcal mol^{-1} (ref 29), is excellent.

At the saddle point, the length of the bonds that are broken (C−H′) and formed (F−H′) increases by only 1.6 and 63%, respectively, indicating that the reaction of the fluorine atom with methane proceeds via an "early" transition state, i.e., it is a reactantlike transition state. This is the expected behavior that would follow from Hammond's postulate,[30] since the reaction is very exothermic. This geometry agrees with the highest-level ab initio, QCISD(T)//QCISD/6-311+G(2df,2pd), results reported by Troya et al.[9] The saddle point has one imaginary frequency. The absolute value of the imaginary part of this frequency is lower in our calculations than the ab initio values, although it is well-known that sometimes ab initio calculations overestimate this value.[31] Moreover, taking into account the flattening of the PES, the small value of $140i$ cm^{-1} seems physically reasonable. The combined effect of potential energy and zero-point energy, i.e., $\Delta H_o^{\ddagger}$, the conventional transition-state enthalpy of activation

TABLE 1: Reactant and Product Properties[a] Calculated Using the Analytical Surface

	CH_4			CH_3			FH		
	PES−SO	PES−N OSO	exp[b]	PES−SO	PES−N OSO	exp[b]	PES−SO	PES−N OSO	exp[b]
				geometr y					
R_{C-H}	1.094	1.094	1.091	1.094	1.094	1.079			
R_{F-H}							0.916	0.916	0.917
				frequen cy					
	3146	3138	3018	3182	3182	3184	4115	4177	4139
	3146	3138	3018	3182	3182	3184			
	3146	3138	3018	3072	3072	3002			
	2984	2978	2916	1380	1380	1383			
	1538	1468	1534	1380	1380	1383			
	1538	1468	1534	580	580	580			
	1344	1286	1306						
	1344	1286	1306						
	1344	1286	1306						
				energy					
ΔH_r[c]	−32.00	−31.80	−32.00						
ZPE	27.92	27.42	27.10	18.27	18.27	18.18	5.88	5.97	5.92

[a] Distances in Å, frequencies in cm^{-1}, energies in kcal mol^{-1}. [b] Experimental data from ref 29. [c] Enthalpy of reaction at 0 K.

TABLE 2: Saddle-Point Properties[a] Calculated at Several Levels

	APES[b]	PES−SO	PES−NOSO	MP4/b1[c]	QCI/b2[d]	QCI/b1[e]
			geometry			
R_{C-H}	1.090	1.094	1.094	1.082	1.089	1.085
$R_{C-H'}$	1.140	1.112	1.107	1.120	1.124	1.114
$R_{F-H'}$	1.373	1.496	1.550	1.458	1.515	1.551
			frequency			
	3126	3133	3127	3254	3188	3201
	3126	3133	3127	3254	3188	3201
	3018	3033	3032	3128	3084	3094
	1913	2580	2711	1979	2206	2389
	1328	1479	1416	1514	1515	1513
	1328	1479	1416	1514	1515	1513
	1198	1264	1221	1284	1305	1298
	1198	1241	1201	1284	1297	1298
	1159	2141	1201	1261	1297	1297
	327	145	119	153	55i	116
	327	145	119	153	55i	116
	318i	140i	106i	578i	578i	283i
			energy			
$\Delta E^{\ddagger}$	1.00	0.51	0.25	1.59	1.44	0.46
$\Delta H^{\ddagger}$ (0 K)	−0.41	−0.43	−0.45	−0.13	−0.36	−0.65
ZPE	25.80	26.98	26.72	26.84	26.58	27.21

[a] Distances in Å, frequencies in cm^{-1}, energies in kcal mol^{-1}. C_{3v} symmetry. [b] Asymmetric surface from our previous work.[1] [c] PUMP4//UMP2/6-311+G(2df,2dp) from ref 9. [d] QCISD(T)//QCISD/6-311+G(2d,p) from ref 9. [e] QCISD(T)//QCISD/6-311+G(2df,2dp) from ref 9.

at 0 K (where the errors between reactants and saddle point have balanced out) is in good agreement with the values predicted by the highest-level ab initio calculations reported to date.[9]

3. Dynamical Calculations

Starting from the saddle point, we followed the reaction path in mass-weighted Cartesian coordinates, obtaining the minimum energy path (MEP).[32] Along this MEP, the reaction coordinate, s, is defined as the signed distance along the MEP from the saddle point, whose s is arbitrarily taken as zero. On the reactant side, $s < 0$, while $s > 0$ on the product side.

Along the MEP we also performed Hessian calculations and a normal-mode analysis in redundant curvilinear coordinates,[33,34] after projecting out from the Hessian the motion along the reaction path.[35] With this information, two important magnitudes can be evaluated. First, the vibrationally adiabatic ground-state potential, $V_a^G(s)$, that can be considered as the free energy along the reaction path at 0 K, and second the coupling terms,[35] $B_{k,F}(s)$, measuring the coupling between the normal mode k and the motion along the reaction coordinate, mode F. These coupling terms control the nonadiabatic flow of energy between these modes and the reaction coordinate.[36,37] These coupling terms will allow us to calculate accurate semiclassical tunneling factors and to give a qualitative explanation of the possible vibrational excitation of reactants and/or products, i.e., dynamical features, which are another sensitive test of the new surface.

In the canonical approach, the variational transition state can be determined by locating the value s^* of s for which the free energy along the reaction path for a temperature T reaches its maximum, $\Delta G(T,s^*)$. We calculated the thermal rates using the improved canonical variational theory (ICVT) approach,[38] given by

$$k^{ICVT}(T) = \min_s \sigma \frac{k_B T}{h} \frac{Q^{GT}(T,s^*)}{Q^R(T)} \exp[-V_{MEP}/k_B T] \quad (4)$$

where k_B and h are Boltzmann's and Planck's constants, respectively, σ is the symmetry factor, taken as 4 for the present reaction, and Q^{GT} and Q^R are the quantal partition functions

for the generalized transition state and the reactants, respectively, where $Q^R(T)$ contains the relative translational partition function per unit volume. The rotational partition functions were calculated classically, and the vibrational modes were treated as quantum mechanical separable harmonic oscillators, with the generalized normal modes defined in redundant curvilinear coordinates.[33,34] As indicated in the previous section, the electronic partition function of the reactants takes the conventional expression in terms of the degeneracy

$$Q_e = 4 + 2\exp(-\epsilon/k_B T) \quad (3)$$

and it is assumed that the electronic partition function of the transition state is two, i.e., it is assumed that the spin−orbit effect is fully quenched in this zone.

The rate constant given by eq 4 is semiclassical, since motion orthogonal to the reaction path is treated quantum mechanically while the motion along the reaction path is classical. To obtain accurate rate constants comparable with experimental values, it is necessary to include quantum mechanical effects in the reaction coordinate motion. This is done by multiplying the semiclassical rate constant by a transmission factor that takes into account tunneling below the barrier and quantum reflection above the barrier. The most complete level of tunneling calculation we employed was the microcanonical optimized multidimensional tunneling (μOMT) approach[39] in which, at each total energy, the larger of the small-curvature (SCT)[40] and large-curvature (LCT) tunneling probabilities is taken as the best estimate. The LCT calculation is based on the large-curvature ground-state approximation, version 4 (LCG4).[41] In the LCT calculations, we allowed the system to reach all the accessible vibrational excited states into which tunneling proceeds.[42]

All the dynamical calculations were performed using the general polyatomic rate constants code POLYRATE.[43] We used the mapped interpolation method[44] to reduce the effect on the final rate constant of the different computational parameters that could affect the numerical accuracy of the resulting semiclassical rate constants and transmission coefficients.

4. Results and Discussion

4.1. Rate Constants for the Isotopically Unsubstituted Reaction. In the improved canonical version of the variational transition-state theory (ICVT), the dividing surface separating reactants from products is located at the maximum of the free-energy curve, at the value $s^{*,ICVT}(T)$. This dynamical bottleneck is located far of the saddle point, ranging from −0.318 bohr at 180 K to +0.304 bohr at 500 K. Thus, the ICVT rate constants differ from those predicted by conventional (nonvariational) transition-state theory (TST), which assumes that the dynamical bottleneck is located at the saddle point ($s = 0$). This effect is known as the "variational effect".

Table 3 lists the variational rate constants (ICVT/μOMT) obtained with the PES−SO surface, together with other theoretical[9] and experimental[17] values for comparison. Figure 1 shows the corresponding Arrhenius plots. The ab initio results of Troya et al.[9] underestimate the experimental data, between 20% at 200 K and 30% at 400 K, showing only a relative agreement with experiment despite the enormous computational effort. The PES−SO rate constants show excellent agreement at high temperatures, with differences of about 2%, but deviate greatly at low temperatures, about 30% at 200 K. Therefore, the variation of the rate constants with temperature does not follow the experimental behavior. Despite the fact that the experimental data were used in the parametrization, all attempts to reproduce the experimental variation with temperature were unsuccessful.

TABLE 3: Forward Thermal Rate Constants for the F + CH_4 Reaction[a]

T(K)	PES−SO	PES−NOSO	ab initio[b]	exp[c]
180	5.58	3.59		3.9
200	5.81	3.97	3.54	4.4
225	6.08	4.41		5.0
250	6.34	4.82	3.96	5.5
275	6.59	5.16		6.0
298	6.82	5.49	4.37	6.3
300	6.84	5.51		6.4
325	7.08	5.88		6.7
350	7.32	6.21		7.0
375	7.57	6.51		7.3
400	7.80	6.82	5.31	7.6
410	7.88	6.93		7.7
500	8.74	8.00	6.06	

[a] ICVT/μOMT rate constants, in 10^{-11} cm^3 molecule^{-1} s^{-1} [b] PUMP4//UMP2/6-311+G(2df,2pd) level from ref 9. [c] Experimental literature revision from ref 17.

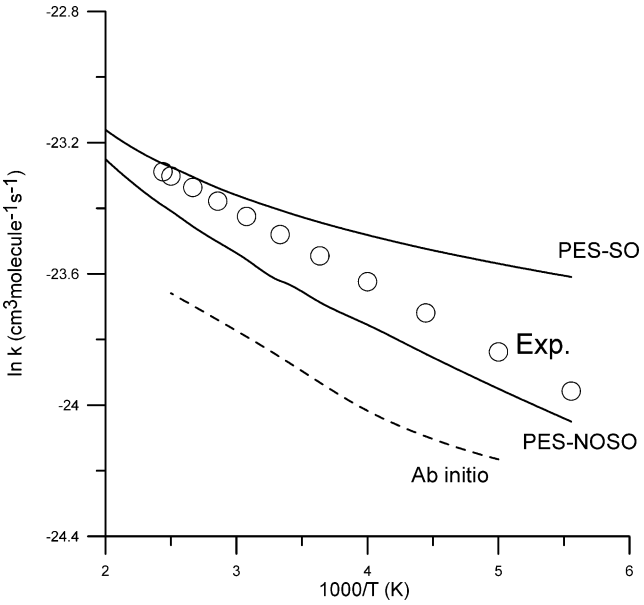

Figure 1. Arrhenius plot of ln k (cm^3 molecule^{-1} s^{-1}) against the reciprocal of the temperature (K) in the range 180−500 K for the forward thermal reaction. Theoretical results: solid line, our ICVT/mOMT values on the PES−SO and PES−NOSO surfaces; dashed line, Troya's values.[9] Experimental results from ref 17 (circles), where the error bars have not been plotted for clarity of the figure.

4.2. Modified Surface. The poor kinetics description with the PES−SO surface means that we have to modify it. Among the possible sources of error (such as deficiencies of the PES, tunneling effect, reactivity of the spin−orbit excited state of the fluorine, etc.) recently Matzkies and Manthe[45] drew attention to the choice of the electronic partition function when the spin−orbit coupling is not considered. They proposed the following expression for the reactants

$$Q_e = 4\exp(\epsilon/3k_B T) + 2\exp(-2\epsilon/3k_B T) \quad (5)$$

i.e., taking now as reference level the average energy of the $^2P_{3/2}$ and $^2P_{1/2}$ states of the fluorine atom, which in this case is $^1/_3\epsilon \approx 0.38$ kcal mol^{-1} above the s−o ground state.

As well as this s−o effect on the multiple electronic states, there is a second effect on the barrier height. In fact, excluding the s−o effect would raise the energy of the s−o ground state of the F by $^1/_3\epsilon \approx 0.38$ kcal mol^{-1} above its relativistic energy,

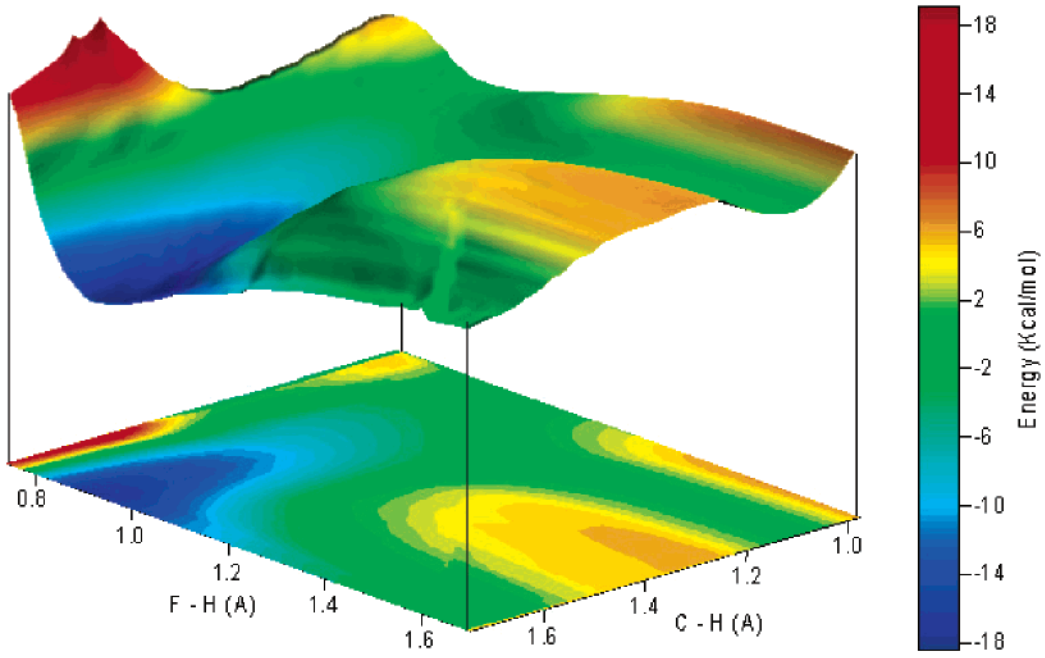

Figure 2. PES−NOSO and contour plots for the gas-phase $CH_4 + F \rightarrow CH_3 + FH$ reaction.

i.e., it would lower the barrier height by this amount. This effect has been considered in the calibration process.

Most recently, Tashiro et al.[46] for the $O(^3P) + O_2$ reaction, and Yagi et al.[47] for the $O(^3P) + CH_3$ reaction, used different electronic partition functions and concluded that which choice is made may lead to non-negligible errors. For the $O(^3P) + O_2$ reaction, for instance, Tashiro et al. found that when the usual Q_e value is used (equivalent to our eq 3) the results overestimate the rate constants, in agreement with our PES−SO results (Figure 1), while when other expressions are used (equivalent to our eq 5) the results underestimate the rate constants.

On the basis of this knowledge, we performed a new calibration using the same functional form but changed the original electronic function partition of the reactants (eq 3) to the expression proposed by Matzkies and Manthe (eq 5). This second surface will be denoted PES−NOSO, adiabatic PES with s−o effect not included, and can also be found on our Web page.[28] A three-dimensional representation and the contour plots are shown in Figure 2. The properties of the reactant and products are listed in Table 1, while those of the saddle point are listed in Table 2. In general, the PES−NOSO surface shows excellent agreement with the results of the stationary points from the PES−SO surface and with the available experimental data (geometry, energy, and frequency). Note that the classical barrier height is higher for the PES−SO surface, which takes as reference level the s−o ground state of the fluorine atom ($^2P_{3/2}$), than for the PES−NOSO surface, as was anticipated in the calibration process.

The rate constants for the new PES−NOSO surface are listed in Table 3 and plotted in Figure 1. The new rate constants reproduce the experimental variation with temperature, being underestimated by about 10% over the whole temperature range. This underestimate has been intentionally considered in the calibration process to take into account the reactivity of the spin−orbit excited state of the fluorine atom ($^2P_{1/2}$) due to nonadiabatic electronic transitions, which for the similar F($^2P_{3/2}$,$^2P_{1/2}$) + H_2 atom+diatom reaction represents about 10−25% of that of the ground state.[27a,c]

First, we shall consider the tunneling factor, which is practically unity over all the temperature range (180−500 K). These values contrast with the theoretical results reported by Troya et al.[9] who, using the calculated adiabatic barrier $\Delta V_a^G = 1.48$ kcal mol^{-1}, obtained values from 4.0 to 1.15 over the same temperature range. However, given the flattening of the PES, it was to be expected that the tunneling factor would be small or negligible, and therefore our results seem physically reasonable.

Second, to provide the most appropriate comparison with experiment, the phenomenological activation energy was computed as the local slope of an Arrhenius plot. Over the common temperature range, 180−410 K, our theoretical result, 0.42 kcal mol^{-1}, closely agrees with experiment,[17] 0.43 kcal mol^{-1}. Note that the PES−SO surface gives a value of 0.22 kcal mol^{-1}, even in agreement with experiment.

4.3. Reaction Path and Coupling Terms. For the PES−NOSO surface, Figure 3 shows the classical potential energy, V_{MEP}, the ground-state vibrationally adiabatic potential-energy curve, ΔV_a^G, and the change in the local zero-point energy, ΔZPE, as a function of s over the range −2.0 to +2.0 bohr. Note that ΔV_a^G and ΔZPE are defined as the difference between V_a^G at s or ZPE at s and their values for reactants.

In this very flat PES, the position of the maximum of ΔV_a^G appears very shifted with respect to the saddle point ($s = 0$), at $s = -1.388$ bohr, in the entrance channel, i.e, the transition state is "early", as it was noticed previously. This shift is known as the "variational effect" and is due to the balance between entropy and energy, where small entropy changes cause large separation of the saddle point location on this very flat surface. The ΔZPE curve drops at about $s = +1.0$ bohr and shows a broad well. This behavior is typical of hydrogen abstraction reactions and the change with s is mainly due to the drop in the CH_4 stretching corresponding to the normal mode breaking during the reaction, which evolves to the FH stretching mode forming in the product (reactive mode).

As we mentioned above, the coupling terms $B_{k,F}(s)$ between the reaction coordinate and the orthogonal bound modes control the nonadiabatic flow of energy between these modes and are a hard test of the new surface. Figure 4 shows these coupling terms as a function of s. We found only two peaks in the exit channel. The larger peak is due to the strong coupling of the

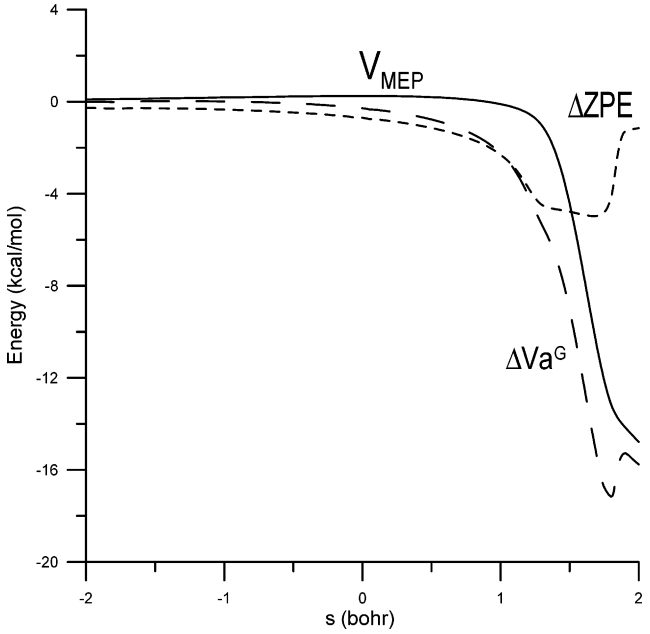

Figure 3. Classical potential-energy curve, V_{MEP}, ΔZPE, and vibrationally adiabatic potential energy curve, ΔV_a^G, as a function of the reaction coordinate *s*. All quantities are with respect to the reactants.

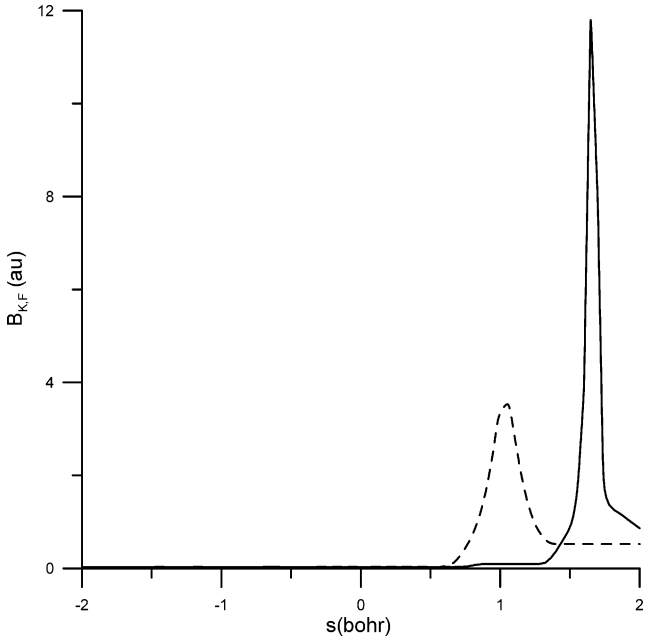

Figure 4. Curvature elements, $B_{k,F}(s)$. Coupling along the MEP between the reaction coordinate (F) and the reactive mode (solid line) and the CH_3 umbrella mode (dashed line).

reaction coordinate to the F−H stretching mode, and the lower ($s = +1.05$ bohr) is due to the coupling to the CH_3 umbrella bending mode. Thus, these two modes could appear vibrationally excited. This dynamic analysis agrees with an "early" transition state, as obtained with this analytical PES, where the products are formed with vibrational excitation.[38,48−50] This description of the coupling terms agrees with those obtained in our previous work with the asymmetric PES (APES),[1] although in those the $B_{k,F}(s)$ term corresponding to methane, i.e., CH_3 umbrella bending in the exit channel, was less pronounced. Finally, it is necessary to indicate that the results obtained with our symmetric PES agree with the available experimental data:[15,26,51] large FH stretching vibrational excitation,[26] and small CH_3[51] (or CD_3)[15] umbrella vibrational excitation in products.

TABLE 4: Kinetic Isotope Effects for the F + CH_4/CD_4

T(K)	PES−SO	PES−NOSO	exp
180	2.17	2.07	
200	2.08	2.01	
225	2.00	1.94	
250	1.93	1.87	
275	1.87	1.81	
283	1.85	1.79	1.9 ± 0.9,[a] 1.7 ± 0.3[b]
298	1.83	1.77	1.4 ± 0.1,[c] 1.5 ± 0.5[d]
300	1.82	1.76	
325	1.78	1.73	
350	1.74	1.70	
375	1.71	1.66	
400	1.67	1.63	
410	1.66	1.62	
500	1.57	1.54	

[a] Reference 52. [b] Reference 53. [c] Reference 26f. [d] Reference 54.

4.4. Kinetic Isotope Effects. Another very sensitive test of several features of the shape of the new surface (barrier height and width and ZPE near the dynamic bottleneck) are the KIEs. This magnitude is defined following the convention that the rate for the lighter isotope is always in the numerator. Hence, a value greater than 1 is considered as a "normal" KIE, while a value less than 1 is an "inverse" KIE. The F + CH_4/CD_4 KIEs are listed in Table 4 for the temperature range 180−500 K, together with the sparse experimental values for comparison.[26f,52−54] The KIEs obtained with the PES−NOSO surface agree reasonably with the corresponding common experimental data at 283 and 298 K, taking into account the large uncertainties of the experimental values. The PES−SO surface KIEs also agree with the experimental values, but in this case due, possibly, to an error cancellation.

4.5. Comparison with the Earlier Asymmetric PES. There are several important differences between the earlier asymmetric PES[1] and this new symmetric surface. With respect to the functional form, while in the earlier PES some terms were not symmetric to all four methane hydrogens; in this new surface, all terms (stretching and bending) are symmetric with respect to the permutation of the four hydrogen atoms in methane, a feature of especial interest for dynamics studies. With respect to the calibration criteria, while in the earlier PES the criterion was to reproduce the experimental properties and electronic structure calculations of the stationary points (geometry, frequency, and changes of energy, reaction, and activation), in this new surface the criterion is to reproduce also the experimental rate constants. In line with the observation in the Introduction that the construction of new PES is a process in continuous evolution, note that in the 1996 PES this experimental magnitude was not included in the calibration process because of the discrepancy between different laboratories. In particular, while Atkinson et al.'s revision data of 1992[2] indicated that the rate constant increased with temperature, the experimental measurement by Moore et al.[3] reported in 1994 showed the opposite behavior. The experimental study by Persky[10] in that same year and the successive revisions[11,12,14,17] since then seem to confirm the earlier results of Atkinson et al.[2] and lend confidence to the most recent values reported to date,[17] which were used in this work. Finally, another important difference is the consideration of the spin−orbit effect. While in the earlier PES the s−o excited state $^2P_{1/2}$ of F ($\epsilon = 404$ cm^{-1}) was included in the electronic partition function, which takes the form $Q_e(F) = 4 + 2\exp(-\epsilon/KT)$; in the present work two versions of the adiabatic PES were considered: the PES−SO surface which uses the same electronic partition function and the PES−NOSO surface which takes into account the correction proposed by Matzkies and

Manthe,[45] $Q_e = 4\exp(\epsilon/3k_BT) + 2\exp(-2\epsilon/3k_BT)$, which takes as reference level the average energy of the $^2P_{3/2}$ and $^2P_{1/2}$ states of F, $^1/_3\epsilon = 0.38$ kcal mol^{-1} above the s−o ground state.

The most important effect of these differences is on the rate constants. We note especially that the shape of the adiabatic curve is similar but with a lower barrier, which is correlated with the lowering of the absolute value of the imaginary frequency, from 318*i* to 140*i* (PES−SO) and 106*i* (PES−NOSO) cm^{-1}, at the saddle point. This behavior now yields KIEs in better agreement with the experimental values.

5. Conclusions

In this work, we have corrected the functional form and recalibrated our previous analytical surface (APES) for the gas-phase $F + CH_4$ reaction. The new surface is now completely symmetric with respect to the permutation of the four methane hydrogen atoms and is calibrated with respect to the updated theoretical and experimental data; therefore, it is semiempirical. Moreover, taking into account that the fluorine atom presents two spin−orbit electronic states split by only $\epsilon = 404$ cm^{-1}, nonadiabatic contributions can contribute to the reaction dynamics, as in the similar and well-studied "benchmark" $F + H_2$ reaction. Within the Born−Oppenheimer approximation, i.e., a single, adiabatic PES, two versions of the surface were considered: the PES−SO version takes as zero reference level the s−o ground state of the fluorine atom ($^2P_{3/2}$), while the PES−NOSO version takes as zero reference level the average energy of the two s−o states, with a value of $^1/_3\epsilon$ above the s−o ground state. As calibration criteria, we used geometrical and energy properties of the stationary points (reactant, products, and saddle point), and experimental thermal rate constants. Both adiabatic surfaces are attractive surfaces, i.e., they present an "early" transition state (reactantlike transition state).

While the PES−SO surface overestimates the experimental rate constants, especially at low temperatures, and does not reproduce the experimental variation with temperature, the PES−NOSO surface shows excellent agreement with the experimental information, taking into account the experimental error bar. This agreement is, obviously, a consequence of the parametrization used, but it lends confidence to the new PES and permits us to obtain the kinetic isotope effects. This surface yields activation energy and KIEs in excellent agreement with the available experimental data, which represents another sensitive test of several features of the new surface.

The analysis of the reaction-path curvature (another dynamics feature) qualitatively showed that large F−H stretching and small CH_3 umbrella vibrational excitations are expected in products. This qualitative dynamics prediction agrees with the experimental evidence.[15,26,51] If the polyatomic $F + CH_4$ system had been considered as a "pseudo atom + diatom" reaction, with the CH_3 group taken as a single particle of mass 15 amu, the small excitation of the CH_3 umbrella mode (3−4% of the total energy from experimental data[15,51]) would have been overlooked.

Acknowledgment. This work was partially supported by the Junta de Extremadura, Spain (Project No. 2PR01A002).

Note Added after ASAP Publication. This article was published ASAP on 1/28/2005. Changes have been made to some of the data in a paragraph in section 2.2. The correct version was posted on 2/4/2005.

References and Notes

(1) Corchado, J. C.; Espinosa-García, J. *J. Chem. Phys.* **1996**, *105*, 3160.
(2) Atkinson, R.; Baulch, D. L.; Cox, R. A.; Hampson, R. F., Jr.; Kerr, J. A.; Troe, J. *J. Phys. Chem. Ref. Data* **1992**, *21*, 1380.
(3) Moore, C. F.; Smith, I. W. M.; Stewart, D. W. A. *Int. J. Chem. Kinet.* **1994**, *26*, 813.
(4) Dömötör, G.; Stachó, L. L.; Bán, M. I. *J. Mol. Struct.* **1998**, *455*, 219.
(5) Kornwitz, H.; Persky, A.; Levine, R. D. *Chem. Phys. Lett.* **1998**, *289*, 125.
(6) Okuno, Y.; Yokoyama, S.; Mashiko, S. *J. Chem. Phys.* **2000**, *113*, 3136.
(7) Natanson, G. *J. Chem. Phys.* **2002**, *117*, 6378.
(8) Fukaya, H.; Morokuma, K. *J. Org. Chem.* **2003**, *68*, 8170.
(9) Troya, D.; Millán, J.; Baños, I.; González, M. *J. Chem. Phys.* **2004**, *120*, 5181.
(10) (a) Persky, A. *J. Phys. Chem.* **1996**, *100*, 689. (b) Persky, A. *Chem. Phys. Lett.* **1998**, *298*, 390 (Erratum, *Chem. Phys. Lett.* **1999**, *306*, 416).
(11) Atkinson, R.; Baulch, D. L.; Cox, R. A.; Hampson, R. F., Jr.; Kerr, J. A.; Rossi, M. J.; Troe, J. *J. Phys. Chem. Ref. Data* **1997**, *26*, 521.
(12) DeMore, W. B.; Sander, S. P.; Golden, D. M.; Hampson, R. F., Jr.; Kurylo, M. J.; Howard, C. J.; Ravishankara, A. R.; Kolb, C. E.; Molina, M. J. *JPL Publication 97−4*; 1997.
(13) Harper, W. H.; Nizkorodov, S. A.; Nesbitt, D. J. *J. Chem. Phys.* **2000**, *113*, 3670.
(14) Atkinson, R.; Baulch, D. L.; Cox, R. A.; Crowley, J. N.; Hampson, R. F., Jr.; Kerr, J. A.; Rossi, M. J.; Troe, J. *NIST report*; 2001.
(15) Zhou, J.; Lin, J. J.; Shiu, W.; Pu, S.-C.; Liu, K. *J. Chem. Phys.* **2003**, *119*, 2538.
(16) Zhou, J.; Lin, J. J.; Shiu, W.; Liu, K. *J. Chem. Phys.* **2003**, *119*, 4997.
(17) Atkinson, R.; Baulch, D. L.; Cox, R. A.; Crowley, J. N.; Hampson, R. F., Jr.; Kerr, J. A.; Rossi, M. J.; Troe, J. *IUPAC Subcommittee on Gas Kinetic Data Evaluation, February*; 2004.
(18) Joseph, T.; Steckler, R.; Truhlar, D. G. *J. Chem. Phys.* **1987**, *87*, 7036.
(19) Jordan, M. J. T.; Gilbert, R. G. *J. Chem. Phys.* **1995**, *102*, 5669.
(20) Espinosa-García, J. *J. Chem. Phys.* **1999**, *111*, 9330.
(21) Espinosa-García, J.; García-Bernáldez, J. *Phys. Chem. Chem. Phys.* **2000**, *2*, 2345.
(22) Corchado, J. C.; Truhlar, D. G.; Espinosa-García, J. *J. Chem. Phys.* **2000**, *112*, 9375.
(23) Espinosa-García, J.; Corchado, J. C. *J. Chem. Phys.* **2000**, *112*, 5731.
(24) Espinosa-García, J. *J. Chem. Phys.* **2002**, *117*, 2076.
(25) Espinosa-García, J. *J. Chem. Phys.* **2002**, *116*, 10664.
(26) (a) Parker, J. H.; Pimentel, G. C. *J. Chem. Phys.* **1969**, *51*, 91. (b) Jonathan, N.; Melliar-Smith, C. M.; Slater, D. H. *Mol. Phys.* **1971**, *20*, 93. (c) Chang, H. W.; Setser, D. W. *J. Chem. Phys.* **1973**, *58*, 2298. (d) Nazar, M. A.; Polanyi, J. C. *Chem. Phys.* **1981**, *55*, 299. (e) Manocha, A. S.; Setser, D. W.; Wickramaaratchi, M. A. *Chem. Phys.* **1983**, *76*, 129. (f) Wickramaaratchi, M. A.; Setser, D. W.; Hildebrant, H.; Korbitzer, B.; Heydtmann, H. *Chem. Phys.* **1985**, *94*, 109. (g) Harper, W. H.; Nizkorodov, S. A.; Nesbitt, D. J. *J. Chem. Phys.* **2000**, *113*, 3670.
(27) (a) Alexander, M. H.; Werner, H.-J.; Manolopoulos, D. E. *J. Chem. Phys.* **1999**, *109*, 4013. (b) Aoiz, F. J.; Bañares, L.; Castillo, J. F. *J. Chem. Phys.* **1999**, *111*, 4013. (c) Alexander, M. H.; Manolopoulos, D. E.; Werner, H.-J. *J. Chem. Phys.* **2000**, *113*, 11084. (d) Aquilanti, V.; Cavalli, S.; Pirani, F.; Volpi, A.; Cappelletti, D. *J. Phys. Chem. A* **2001**, *105*, 2401. (e) Aquilanti, V.; Cavalli, S.; De Fazio, D.; Volpi, A.; Aguilar, A.; Gimenez, X.; Lucas, J. M. *Phys. Chem. Chem. Phys.* **2002**, *4*, 401. (f) Aquilanti, V.; Cavalli, S.; De Fazio, D.; Volpi, A.; Aguilar, A.; Gimenez, X.; Lucas, J. M. *Chem. Phys. Lett.* **2003**, *371*, 504. (g) Zhang, Y.; Xie, T.-X.; Han, K.-L.; Zhang, J. Z. H. *J. Chem. Phys.* **2003**, *119*, 12921.
(28) http://w3qf.unex.es/html/superficies.htm.
(29) *JANAF Thermochemical Tables*, 3rd ed.; Chase, M. W., Jr., Davies, C. A., Downey, J. R., Frurip, D. J., McDonald, R. A., Syverud, A. N., Eds.; National Bureau of Standards: Washington, DC, 1985; Vol. 14.
(30) Hammond, G. S. *J. Am. Chem. Soc.* **1955**, *77*, 334.
(31) Hehre, W. J.; Radom, L.; Schleyer, P.v.R.; Pople, J. A. *Ab initio Molecular Orbital Theory*; Wiley: NY, 1989.
(32) Allison, T. C.; Truhlar, D. G. In *Modern Methods for Multidimensional Dynamics Computations in Chemistry*; Thompson, D. L., Ed.; World Scientific: Singapore, 1998.
(33) Jackels, C. F.; Gu, Z.; Truhlar, D. G. *J. Chem. Phys.* **1995**, *102*, 3188.
(34) Chuang, Y. Y.; Truhlar, D. G. *J. Phys. Chem.* **1997**, *101*, 3808.
(35) Miller, W. H.; Handy, N. C.; Adams, J. E. *J. Chem. Phys.* **19980**, *72*, 99.
(36) Morokuma, K.; Kato, S. In *Potential Energy Surfaces and Dynamics Calculations*; Truhlar, D. G., Ed.; Plenum: New York, 1981; p 243.
(37) Kraka, E.; Dunning, T. H. In *Advances in Molecular Electronic Structure Theory*; JAI, New York, 1990; Vol. I, p 129.

(38) Truhlar, D. G.; Isaacson, A. D.; Garrett, B. C. In *The Theory of Chemical Reactions*; Baer, M., Ed.; Chemical Rubber: Boca Raton, FL, 1985; Vol. 4.
(39) Liu, Y.-P.; Lu, D.h.; González-Lafont, A.; Truhlar, D. G.; Garrett, B. C. *J. Am. Chem. Soc.* **1993**, *115*, 7806.
(40) Lu, D.h.; Truong, T. N.; Melissas, V. S.; Lynch, G. C.; Liu, Y. P.; Garrett, B. C.; Steckler, R.; Isaacson, A. D.; Rai, S. N.; Hancock, G. C.; Lauderdale, G. C.; Joseph, T.; Truhlar, D. G. *Comput. Phys. Commun.* **1992**, *71*, 235.
(41) Fernández-Ramos, A.; Truhlar, D. G. *J. Chem. Phys.* **2001**, *114*, 1491.
(42) Truong, T. N.; Lu, D.h.; Lynch, G. C.; Liu, Y. P.; Melissas, V. S.; Stewart, J. J.; Steckler, R.; Garrett, B. C.; Isaacson, A. D.; González-Lafont, A.; Rai, S. N.; Hancock, G. C.; Joseph, T.; Truhlar, D. G. *Comput. Phys. Commun.* **1993**, *75*, 43.
(43) Chuang, Y. Y.; Corchado, J. C.; Fast, P. L.; Villa, J.; Coitino, E. L.; Hu, W. P.; Liu, Y. P.; Lynch, G. C.; Nguyen, K. A.; Jackels, C. F.; Gu, M. Z.; Rossi, I.; Clayton, S.; Melissas, V. S.; Steckler, R.; Garrett, B. C.; Isaacson, A. D.; Truhlar, D. G. *POLYRATE-version 8.4*; University of Minnesota: Minneapolis, 1999.
(44) Corchado, J. C.; Coitiño, E. L.; Chuang, Y. Y.; Fast, P. L.; Truhlar, D. G. *J. Phys. Chem. A* **1998**, *102*, 2424.
(45) Matzkies, F.; Manthe, U. *J. Chem. Phys.* **1998**, *108*, 4828.
(46) Tashiro, M.; Schinke, R. *J. Chem. Phys.* **2003**, *119*, 10186.
(47) Yagi, K.; Takayanagi, T.; Taketsugu, T.; Hirao, K. *J. Chem. Phys.* **2004**, *120*, 10395.
(48) Polanyi, J. C.; Wong, W. H. *J. Chem. Phys.* **1969**, *51*, 1439.
(49) Perry, D. S.; Polanyi, J. C.; Wilson, C. W. *J. Chem. Phys.* **1974**, *53*, 317.
(50) Duff, J. W.; Truhlar, D. G. *J. Chem. Phys.* **1975**, *62*, 2477.
(51) Sugawara, K.; Ito, F.; Nakanaga, T.; Takeo, H.; Matsumura, Ch. *J. Chem. Phys.* **1990**, *92*, 5328.
(52) Foon, R.; Reid, G. P.; Tait, K. B. *J. Chem. Soc., Faraday Trans.* **1972**, *68*, 1131.
(53) Williams, R. L.; Rowland, F. S. *J. Phys. Chem.* **1973**, *77*, 301.
(54) Wallington, T. J.; Hurley, M. D. *Chem. Phys. Lett.* **1992**, *193*, 84.